Available online at www.sciencedirect.com
SCIENCE DIRECT®
PERGAMON
International Journal of Heat and Mass Transfer 46 (2003) 2263–2277
International Journal of HEAT and MASS TRANSFER
www.elsevier.com/locate/ijhmt

Stability analysis of the perturbed rest state and of the finite amplitude steady double-diffusive convection in a shallow porous enclosure

Mahmoud Mamou *

Institute for Aerospace Research, National Research Council Canada, Ottawa, Ontario, Canada K1A 0R6

Received 4 March 2002; received in revised form 17 September 2002

Abstract

Transition from rest and steady convective states to oscillatory flows is investigated in a shallow porous enclosure subject to vertical thermal and solutal gradients. Various combinations of Dirichlet and Neumann thermal and solutal boundary conditions is considered. The unsteady form of Hazen–Darcy law with the Boussinesq approximation is used to model the convective flow through the porous medium. The governing and perturbation equations are solved numerically using finite element method. The threshold of transition, which characterizes the transition from steady to oscillatory finite amplitude flows, and the threshold of overstability (Hopf bifurcation), which characterizes the transition from the rest to oscillatory state, are obtained for a wide range of the governing parameters. The porosity and the acceleration parameter of the porous medium have a strong effect on the thresholds of transition and overstability. An increase in the acceleration parameter and the normalized porosity delays the onset of overstability and the transition to oscillatory finite amplitude flows. For Neumann boundary conditions type, the wavenumber is zero at the onset of overstabilities and finite at the transition threshold.

Keywords: Porous layer; Overstabilities; Transition; Mixed boundary conditions; Stability analysis; Finite element method

1. Introduction

Combined heat and mass transfer by natural convection in porous materials is a field of great interest for many researchers and engineers. Its applications include many diversified fields such as transport of moisture in fibrous insulation and contaminants in saturated soil. Underground disposal of nuclear or non-nuclear wastes, food processing, metallurgy and chemistry are also some disciplines where combined heat and solute transfer in multi-component fluids are involved.

In double-diffusive convection, when the thermal and solutal buoyancy forces are comparable and opposing each other, a rich variety of phenomena can occur (here, the word solutal refers to solute or mass transfer effects). These phenomena include the possible existence of multiple steady and unsteady state solutions for the same set of governing parameters, subcritical and oscillatory flows, traveling waves and asymmetric flow patterns (see, for example, Nield [1], Taunton et al. [2], Mamou et al. [3] and Mamou and Vasseur [4]). These convective phenomena are caused by the fact that the thermal and solutal diffusivities are different from each other, which leads to different time scales for the heat and solute transfer. Therefore, the heat and solute transfers can get out of phase and cause the different convective phenomena mentioned above. The difference in time scales can also occur when the solid material of the porous medium

* Tel.: +1-613-998-9953; fax: +1-613-998-1281.
E-mail address: Mahmoud.Mamou@nrc-cnrc.gc.ca (M. Mamou).

0017-9310/03/$ - see front matter
doi:10.1016/S0017-9310(02)00523-9

Nomenclature

A	aspect ratio, W'/H'
a	integer, equals 0 for Dirichlet boundary conditions and 1 for Neumann
A_C	critical wavelength
Da	Darcy number, K/H'^2
g	acceleration due to gravity
H'	thickness of the porous layer
j'	constant solute flux
k	wavenumber
N	Buoyancy ratio, $R_S/(R_T Le)$
Nu	Nusselt number
Pr	Prandtl number
q'	constant heat flux
R_T	thermal Rayleigh number, $g\beta_T \Delta T^* KH'/(\alpha_T \nu)$
R_S	solutal Rayleigh number, $g\beta_S \Delta S^* KH'/(\alpha_S \nu)$
R_{TC}^{sub}	subcritical critical Rayleigh number
R_{TC}^{over}	overstable critical Rayleigh number
R_{TC}^{sup}	supercritical Rayleigh number
R_{TC}^{tran}	critical Rayleigh number for transition
Sh	Sherwood number
S	dimensionless solute concentration, $(S' - S'_0)/\Delta S^*$
ΔS^*	characteristic solute concentration difference
T	dimensionless temperature, $(T' - T'_U)/\Delta T^*$
ΔT^*	characteristic temperature difference
t	dimensionless time, $t'\alpha/(\sigma H'^2)$
W'	length of the porous layer
x, y	dimensionless coordinates system, $(x'/H', y'/H')$

Greek symbols

α	diffusivity coefficient
β	expansion coefficient
ϵ	porosity of the porous medium
ε	normalized porosity of the porous medium
κ	thermal conductivity of the saturated porous medium
ν	kinematic viscosity of fluid
ξ	acceleration parameter of the porous medium, $Da/(\sigma\epsilon Pr)$
ρ	density of fluid
$(\rho c)_f$	heat capacity of fluid
$(\rho c)_s$	heat capacity of the saturated porous medium
σ	heat capacity ratio, $\sigma = (\rho c)_s/(\rho c)_f$
Ψ	stream function

Subscripts

0	refers to reference state
L	refers to lower boundary
m	refers to average value
T	refers to thermal
S	refers to solutal
U	refers to upper boundary

is impermeable. The heat transfer is transferred through both the fluid and the solid regions. However, the solute is transported only through the fluid region by diffusion and convection. Thus, the porosity of the porous medium can have a strong effect on the transient flow behavior within the porous medium, even when the thermal and solutal diffusivities are equal.

Double-diffusive convection instabilities in a horizontal porous layer is studied primarily by Nield [1]. The critical Rayleigh numbers for the onset of stationary and overstable convection are obtained for different thermal and solutal boundary conditions using a linear stability analysis. The analysis is extended by Taunton et al. [2]. The conditions for which salt fingers develop are determined. Rudraiah et al. [5] examine a porous layer with isothermal and isosolutal boundaries using a weakly non-linear stability analysis. The effect of the Prandtl number, ratio of thermal and solute diffusivities and permeability parameter on the finite amplitude flow are studied for opposing buoyancy forces. By deriving an asymptotic steady solution, the threshold for subcritical convection is obtained as function of the ratio of diffusivities. Brand and Steinberg [6] investigate finite amplitude convection near the threshold for both stationary and overstable convection. The temporal evolution of the heat and mass transfer rates is predicted.

Numerical and experimental investigations on double-diffusive convection are conducted by Murray and Chen [7] in a horizontal porous layer. The authors find that when solute is stabilizing, the onset of convection is marked by an abrupt increase in the heat flux at a critical temperature difference value. Furthermore, when the temperature difference was reduced below the critical value, the heat flux curve establishes a hysteresis loop, which indicates clearly the existence of subcritical flows. Double-diffusive fingering convection in a horizontal porous layer is considered by Chen and Chen [8]. The boundaries that separate regions of different types of convective modes are identified in terms of the thermal and solutal Rayleigh numbers.

Mamou et al. [3] consider double-diffusive convection in an inclined porous layer subjected to vertical fluxes of heat and solute. For the horizontal layer, their analytical and numerical results show mutual agreement and demonstrates that subcritical steady flows are possible. Studying the same problem within a horizontal porous enclosures, Mamou and Vasseur [4] considers different boundary conditions for temperature and solute concentration. Different convective states are found to coexist below the threshold of stationary convection. General expressions for the thresholds of subcritical, overstable and stationary convective flows are obtained as functions of the governing parameters. Amahmid et al. [9] consider double-diffusive convection in horizontal sparsely packed porous systems subject to vertical fluxes of heat and solute. The threshold for the onset of subcritical and stationary flows are determined as functions of the Darcy number. Mahidjiba et al. [10] examine the effect of mixed thermal and solutal boundary conditions on the thresholds of overstabilities and stationary convection. They demonstrate that when the thermal and solutal effects are opposing each other, the flow patterns become different from the classical Bénard convective flow patterns. Considering the case of Mamou and Vasseur [4], Kalla et al. [11] study the effect of lateral heating on bifurcation phenomena. The authors find that lateral heating acts as an imperfection brought to the bifurcation curves. Multiple steady-state solutions with different heat and mass transfer rates are found to coexist.

The present study describes a thorough investigation of the stability analysis of convective flows within horizontal porous enclosures subject to vertical thermal and solutal gradients. This study is an extension to the previous work conducted by Mamou and Vasseur [4] and Mahidjiba et al. [10] by considering the effect of the acceleration (or inertia) parameter and the normalized porosity of the porous medium on the onset of overstabilities and transition (transition from finite amplitude steady flow to oscillatory flow). The threshold of transition is determined by performing a linear stability analysis of the perturbed steady convective state. For comparison, a finite element solution of the full governing equations is obtained and the effects of the governing parameters on the flow behavior is studied. New expressions for the thresholds of stationary convection are obtained for mixed thermal and solutal boundary conditions. The rich variety phenomena existing in opposing double-diffusive convection and the lack of results on transition phenomenon, which is regarded as the early stage of turbulence, have motivated the present study.

2. Mathematical formulation

The present investigation is on double-diffusive convection instability in horizontal porous enclosure of thickness H' and length W' subject to vertical gradients of temperature and solute. The vertical gradients are established by maintaining the two horizontal boundaries at constant temperatures and concentrations (Dirichlet boundary conditions type) or by imposing constant uniform fluxes of heat and solute to the horizontal boundaries (Neumann boundary conditions type). When the thermal and solutal boundary conditions are of the same type (Dirichlet or Neumann), they are termed as similar boundary conditions, however, when considering Dirichlet thermal and Neumann solutal boundary conditions or vice versa, they are termed as mixed boundary conditions. The vertical walls of the enclosure are kept adiabatic and impermeable.

Adopting Hazen–Darcy law and assuming a Boussinesq incompressible flow, the dimensionless governing equations are given by

$$\xi \frac{\partial(\nabla^2 \Psi)}{\partial t} + \nabla^2 \Psi = -\left(R_T \frac{\partial T}{\partial x} + \frac{R_S}{Le} \frac{\partial S}{\partial x} \right), \tag{1}$$

$$\frac{\partial T}{\partial t} - J(\Psi, T) = \nabla^2 T, \tag{2}$$

$$\varepsilon \frac{\partial S}{\partial t} - J(\Psi, S) = \frac{1}{Le} \nabla^2 S, \tag{3}$$

where Ψ, T and S are the dimensionless stream function, temperature and concentration, respectively. The Jacobian J is defined as $J(\mathrm{f}, \mathrm{g}) = (\partial \mathrm{f}/\partial x)(\partial \mathrm{g}/\partial y) - (\partial \mathrm{f}/\partial y)(\partial \mathrm{g}/(\partial x)$.

The governing equations were non-dimensionalized using the following variables:

$$x = \frac{x'}{H'}, \quad y = \frac{y'}{H'}, \quad t = \frac{t'\alpha_T}{\sigma H'^2}, \quad \Psi = \frac{\Psi'}{\alpha_T}, \quad T = \frac{(T' - T'_0)}{\Delta T^*}, \quad S = \frac{(S' - S'_0)}{\Delta S^*}. \tag{4}$$

Other definitions are as follows:

$$\left.\begin{aligned} T'_0 &= a_T T'_{(0,0)} + (1 - a_T)\frac{T'_L + T'_U}{2}, \quad \Delta T^* = a_T \frac{q' H'}{\kappa} + (1 - a_T)(T'_L - T'_U), \\ S'_0 &= a_S S'_{(0,0)} + (1 - a_S)\frac{S'_L + S'_U}{2}, \quad \Delta S^* = a_S \frac{j' H'}{\alpha_S} + (1 - a_S)(S'_L - S'_U), \end{aligned}\right\} \tag{5}$$

where the subscript $(0,0)$ refers to the origin of the coordinate system, which is at the center of the enclosure with x-axis horizontal and y-axis opposing the gravity). The parameters $(a_T, a_S) = (0,0)$ for Dirichlet boundary conditions and $(a_T, a_S) = (1,1)$ for Neumann boundary conditions. For mixed boundary conditions $(a_T, a_S) = (1,0)$ or $(0,1)$.

The dimensionless boundary conditions are:

$$x = \pm\frac{A}{2}, \quad \Psi = 0, \quad \frac{\partial T}{\partial x} = 0; \quad y = \pm\frac{1}{2}, \quad \Psi = 0, \quad a\frac{\partial \varphi}{\partial y} \pm (1 - a)\varphi = -\frac{a+1}{2}, \tag{6}$$

where a stands for a_T and a_S, and φ for T and S.

The dimensionless governing parameters are the thermal Darcy–Rayleigh number, R_T, the solutal Rayleigh number, R_S, the Lewis number, Le, the enclosure aspect ratio, A, and the normalized porosity, ε. They are defined as follows:

$$R_T = \frac{g\beta_T \Delta T^* K H'}{\alpha_T \nu}, \quad R_S = \frac{g\beta_S \Delta S^* K H'}{\alpha_S \nu}, \quad Le = \frac{\alpha_T}{\alpha_S}, \quad \varepsilon = \frac{\epsilon}{\sigma}, \quad \xi = \frac{Da}{\epsilon \sigma Pr}, \quad A = \frac{W'}{H'}, \tag{7}$$

where $Da = (K/W'^2)$ is the Darcy number.

The local heat and mass transfer rates are given in terms of the local Nusselt and Sherwood numbers:

$$\left.\begin{aligned} Nu &= \frac{a_T}{T_{(x,-1/2)} - T_{(x,1/2)}} + (1 - a_T)\frac{\partial T}{\partial y}\Big|_{y=\pm 1/2}, \\ Sh &= \frac{a_S}{S_{(x,-1/2)} - S_{(x,1/2)}} + (1 - a_S)\frac{\partial S}{\partial y}\Big|_{y=\pm 1/2}, \end{aligned}\right\} \tag{8}$$

and the overall Nusselt and Sherwood number along the horizontal walls can be obtained from:

$$Nu_m = \frac{1}{A}\int_{-A/2}^{A/2} Nu\,\mathrm{d}x \quad \text{and} \quad Sh_m = \frac{1}{A}\int_{-A/2}^{A/2} Sh\,\mathrm{d}x. \tag{9}$$

3. Numerical solution

The full governing equations (1)–(3), with the boundary conditions, (6), are solved using a finite element method. The flow domain is discretized into Lagrange cubic elements, each with nine nodes. The Galerkin weak formulation is obtained first, and then the Bubnov–Galerkin procedure is used to discretize the governing equations using an implicit scheme. Global matrix systems of linear equations are obtained and solved iteratively. Further details regarding the finite element method and the validation of the numerical simulation can be found in Mamou et al. [12,13].

4. Linear stability analysis

The stability of the basic solution is studied in this section. First, the convective solution is decomposed as follows:

$$(\Psi, T, S)_{(t,x,y)} = (\Psi_b, T_b, S_b)_{(x,y)} + (\psi, \theta, \phi)_{(t,x,y)}, \tag{10}$$

where Ψ_b, T_b and S_b is the basic solution that represents the pure diffusive state ($\Psi_b = 0$, $T_b = S_b = -y$) or the steady-state convective solution. The variables ψ, θ and ϕ describe the perturbation profiles imposed on the basic solution. The boundary conditions for the perturbation are:

$$x = \pm\frac{A}{2}, \quad \psi = 0, \quad \frac{\partial\varphi}{\partial x} = 0; \quad y = \pm\frac{1}{2}, \quad \psi = 0, \quad a\frac{\partial\varphi}{\partial y} + (1-a)\varphi = 0, \tag{11}$$

where a stands for a_T and a_S, and φ for θ and ϕ.

Assuming separable variables, the perturbations profiles are given by

$$\psi(x,y,t) = e^{pt+ikx}F(y), \quad \theta(x,y,t) = e^{pt+ikx}G(y), \quad \phi(x,y,t) = e^{pt+ikx}H(y), \tag{12}$$

where $k = n\pi/A$ is the wavenumber and n is the number of cells. For a confined enclosure, $n = 1, 2, 3, \ldots$; for an infinite layer, $n = 2$ with a critical wavelength $A = A_C$.

Upon substituting Eq. (10) into the governing equations (1)–(3) and neglecting the second-order terms, the linearized governing equations are:

$$\left.\begin{aligned}
&(\xi p+1)\left(\frac{d^2F}{dy^2} - k^2F\right) = -ik\left(R_T G + \frac{R_S}{Le}H\right),\\
&pG - \frac{\partial\Psi_b}{\partial x}\frac{dG}{dy} + ik\frac{\partial\Psi_b}{\partial y}G - ikF\frac{\partial T_b}{\partial y} + \frac{dF}{dy}\frac{\partial T_b}{\partial x} = \frac{d^2G}{dy^2} - k^2G,\\
&\varepsilon pH - \frac{\partial\Psi_b}{\partial x}\frac{dH}{dy} + ik\frac{\partial\Psi_b}{\partial y}H - ikF\frac{\partial S_b}{\partial y} + \frac{dF}{dy}\frac{\partial S_b}{\partial x} = \frac{1}{Le}\left(\frac{d^2H}{dy^2} - k^2H\right).
\end{aligned}\right\} \tag{13}$$

The integral Galerkin technique is used to obtain a weak formulation of Eq. (13). Using the finite element method, the discretized linear equations, after assembling into global matrix system, are obtained as follows:

$$\begin{bmatrix} [\mathbf{K}_\psi] & -R_T[\mathbf{B}_\psi] & -\frac{R_S}{Le}[\mathbf{B}_\psi] \\ [\mathbf{B}_\theta] & [\mathbf{K}_\theta] & 0 \\ [\mathbf{B}_\phi] & 0 & \frac{1}{Le}[\mathbf{K}_\phi] \end{bmatrix} \begin{Bmatrix} \mathbf{F} \\ \mathbf{G} \\ \mathbf{H} \end{Bmatrix} = p \begin{bmatrix} -\xi[\mathbf{M}_\psi] & 0 & 0 \\ 0 & -[\mathbf{M}_\theta] & 0 \\ 0 & 0 & -\varepsilon[\mathbf{M}_\phi] \end{bmatrix} \begin{Bmatrix} \mathbf{F} \\ \mathbf{G} \\ \mathbf{H} \end{Bmatrix}, \tag{14}$$

where $[\mathbf{B}_\psi]$, $[\mathbf{B}_\theta]$, $[\mathbf{B}_\phi]$, $[\mathbf{M}_\psi]$, $[\mathbf{M}_\theta]$, $[\mathbf{M}_\phi]$, $[\mathbf{K}_\theta]$, $[\mathbf{K}_\phi]$ and $[\mathbf{K}_\psi]$ are square matrices of dimension $m \times m$, where $m = 2N_{ey} + 1$ (N_{ey} is the number of element in y-direction) is the node number within the domain $\Omega = \{y \in [-1/2, 1/2]\}$. The vectors $\mathbf{F}$, $\mathbf{G}$ and $\mathbf{H}$ are unknown eigenvectors of dimension m. The corresponding elementary matrices are obtained as follows:

$$\left.\begin{aligned}
[B_\psi]^e &= \int_{\Delta y_e} ik\mathscr{L}_j\mathscr{L}_i\,dy,\\
[B_\theta]^e &= \int_{\Delta y_e}\left(\frac{\partial T_b}{\partial x}\frac{d\mathscr{L}_j}{dy} - ik\frac{\partial T_b}{\partial y}\mathscr{L}_j\right)\mathscr{L}_i\,dy,\\
[B_\phi]^e &= \int_{\Delta y_e}\left(\frac{\partial S_b}{\partial x}\frac{d\mathscr{L}_j}{dy} - ik\frac{\partial S_b}{\partial y}\mathscr{L}_j\right)\mathscr{L}_i\,dy,\\
[K_\psi]^e &= \int_{\Delta y_e}\left(\frac{d\mathscr{L}_j}{dy}\frac{d\mathscr{L}_i}{dy} + k^2\mathscr{L}_j\mathscr{L}_i\right)dy,\\
[K_\theta]^e &= \int_{\Delta y_e}\left(\frac{d\mathscr{L}_j}{dy}\frac{d\mathscr{L}_i}{dy} + k^2\mathscr{L}_j\mathscr{L}_i + ik\frac{\partial\psi_b}{\partial y}\mathscr{L}_j\mathscr{L}_i - \frac{\partial\psi_b}{\partial x}\frac{d\mathscr{L}_j}{dy}\mathscr{L}_i\right)dy,\\
[K_\phi]^e &= \int_{\Delta y_e}\left(\frac{d\mathscr{L}_j}{dy}\frac{d\mathscr{L}_i}{dy} + k^2\mathscr{L}_j\mathscr{L}_i + ikLe\frac{\partial\psi_b}{\partial y}\mathscr{L}_j\mathscr{L}_i - Le\frac{\partial\psi_b}{\partial x}\frac{d\mathscr{L}_j}{dy}\mathscr{L}_i\right)dy,\\
[M_\psi]^e &= \int_{\Delta y_e}\left(\frac{d\mathscr{L}_j}{dy}\frac{d\mathscr{L}_i}{dy} + k^2\mathscr{L}_j\mathscr{L}_i\right)dy,\\
[M_\theta]^e &= [\mathbb{M}_\phi]^e = \int_{\Delta y_e}\mathscr{L}_j\mathscr{L}_i\,dy,
\end{aligned}\right\} \tag{15}$$

where $\mathscr{L}_i(y)$ is a one-dimensional Lagrange interpolation functions.

4.1. Stability analysis of the diffusive state

The stability of the rest state ($\Psi_0 = 0$, $T_b = S_b = -y$) is now considered.

4.1.1. Onset of stationary convection

For stationary convection, $p = 0$, the linear global system, Eq. (14), can be arranged to yield the following eigenvalue problem:

$$[E - \lambda I]\{\mathbf{F}\} = 0 \quad \text{with } [E] = [K_\psi]^{-1}[B_\psi][[K_\theta]^{-1}[B_\theta] + NLe[K_\phi]^{-1}[B_\phi]] \quad \text{and} \quad \lambda = \frac{1}{R_T}. \tag{16}$$

Eq. (16) has a non-trivial solution, ($\{\mathbf{F}\} \neq 0$), if and only if the determinant of $[[E] - \lambda[I]]$ is equal to zero, where $[I]$ is the identity matrix. Solving $|[E] - \lambda[I]| = 0$, we obtain m eigenvalues that are classified as $\lambda_1 \leqslant \lambda_2 \leqslant \cdots \leqslant \lambda_{m-1} \leqslant \lambda_m$, where λ_1 is the minimum eigenvalue and λ_m the maximum eigenvalue. The corresponding eigenfunctions are given by $\{\mathbf{F}\}_i$. The eigenvalues are computed using subroutines from the IMSL library.

In general, the maximum eigenvalue, λ_m, is positive and represents the lowest critical thermal Rayleigh number above which the stationary convection is possible. The minimum eigenvalue, λ_1, is usually zero or negative and represents the highest critical thermal Rayleigh number below which convective flow is possible. This situation corresponds to $R_T < 0$, i.e. $\Delta T^* < 0$.

The stream function field at the onset of convection is given by

$$\pm\{\mathbf{F}\}_1 \quad \text{when } \Delta T^* < 0, \quad \text{or } \pm\{\mathbf{F}\}_m \quad \text{when } \Delta T^* > 0. \tag{17}$$

The temperature and concentration fields are obtained from:

$$\{\mathbf{G}\}_i = [K_\theta]^{-1}[B_\theta]\{\mathbf{F}\}_i, \quad \{\mathbf{H}\}_i = Le[K_\phi]^{-1}[B_\phi]\{\mathbf{F}\}_i. \tag{18}$$

4.1.2. Discussion

Typical values of the supecritical Rayleigh number are presented in Table 1 for different boundary conditions and grid sizes. The results are obtained with $N = -1$ and $Le = 2$. Since the Lewis number is specified here, the minimum eigenvalue (as discussed earlier) corresponds to the maximum Rayleigh number below which convection is possible (i.e. $\Delta T^* < 0$). The maximum eigenvalue corresponds to the minimum Rayleigh number above which convection is possible (i.e. $\Delta T^* > 0$). For similar boundary conditions ($a_T = a_S$), the maximum critical value is infinity such that, for $Le = 2$ in the absence of overstability, the pure diffusive state is unconditionally stable. This situation corresponds to $\Delta T^* > 0$ (heating from below). However, the minimum value (−39.479 for $a_T = a_S = 0$, or −22.946 for $a_T = a_S = 1$) corresponds to the critical Rayleigh number when heating from the top. For this situation, the heat is the stabilizing agent and the solute is the destabilizing agent. Similar results are obtained for $(a_T, a_S) = (0, 1)$. However, for $(a_T, a_S) = (1, 0)$, heating from the bottom or from the top, the threshold for stationary convection is finite. For $a_T = a_S = 0$, the critical value agrees well with the known classical value for pure thermal convection, $4\pi^2$.

4.1.3. Onset of overstabilities

Overstabilities set in at a threshold $R_T = R_{TC}^{over}$ beyond which the perturbations grow in an oscillatory manner. The perturbation growth rate parameter ($p = p_r + ip_i$) is a pure complex number. At the onset of overstabilities, $p_r = 0$ and $p_i \neq 0$. The eigenvalue system in Eq. (14) is solved using the subroutine from the IMSL library. For a given set of governing parameters, R_S, Le, A, ε, ξ, a_T and a_S, the eigenvalues, p, and eigenfunctions, $\mathbf{F}$, $\mathbf{G}$ and $\mathbf{H}$ are computed for different thermal Rayleigh numbers, R_T, (for finite aspect ratio enclosure, A) and different wavelengths (for an infinite layer). For a given aspect ratio or wavelength, the threshold at the onset of overstabilities is obtained by observing when the real part changes from a negative to positive value in only one eigenvalue. If the imaginary part of the eigenvalue is non-zero, then the instability is oscillatory. For an infinite layer, the minimum (critical) Rayleigh number is obtained for different wavelengths. The minimum Rayleigh number for all wavelengths represents the threshold of overstabilities,

Table 1
Supercritical Rayleigh number, R_{TC}^{sup} (minimum and maximum values), and grid size effect for the onset of stationary convection within a square enclosure with $Le = 2$ and $N = -1$ and different thermal and solutal boundary conditions

	N_{ey}			
(a_T, a_S)	4	8	12	16
(0, 0)	−39.518, ∞	−39.481, ∞	−39.479, ∞	−39.479, ∞
(1, 1)	−22.975, ∞	−22.948, ∞	−22.946, ∞	−22.946, ∞
(0, 1)	−16.060, ∞	−16.033, ∞	−16.032, ∞	−16.031, ∞
(1, 0)	325.718, −70.449	308.025, −69.695	307.103, −69.650	306.948, −69.642

Table 2
Critical Rayleigh number, R_{TC}^{over}, and oscillation frequency, $fr = |p_i|/2\pi$, for the onset of overstabilities in a square enclosure with $N = -1$, $Le = 2$, $\varepsilon = 0.2$, $\xi = 0$, and $a_T = a_S = 0$

Grid size	2	4	8	10	Nield [1]
R_{TC}^{over}	34.55925	34.54403	34.54363	34.54362	$3.5\pi^2 = 34.5436$
f_r	1.75666	1.75621	1.75620	1.75620	1.75620

and the corresponding aspect ratio is the critical wavelength. At $R_T = R_{TC}^{over}$, two complex conjugate eigenvalues exist. The flow patterns of these two solutions are similar or mirror images of each other.

4.1.4. Discussion

For validation, of the present numerical technique, a square enclosure subject to Dirichlet boundary conditions ($a_T = a_S = 0$) is considered. For this situation, Nield [1] obtained an analytical exact solution for the threshold of overstability. Results obtained for different grid sizes with $N = -1$, $\xi = 0$, $A = 1$ and $a_T = a_S = 0$ are given in Table 2. The results are presented in terms of the threshold for the onset of overstabilities, R_{TC}^{over}, and oscillation frequency, f_r. When the number of grid points increases, the results converge to those obtained by Nield [1]. An efficient way to determine the critical point without excessive computations is to interpolate the critical value between negative p_r^- and positive p_r^+ values of p_r. The variation of p_r with R_T is nearly linear, and thus a first-order interpolation is sufficient without loss of accuracy. Results with high precision are obtained by reducing the gap between p_r^- and p_r^+ (i.e. $|p_r^+ + p_r^-| \to 0$).

With similar thermal and solutal boundary conditions ($a_T = a_S$), the threshold of overstabilities is determined by Nield [1]. Taunton et al. [2] extend the work of Nield by introducing inertial effects (the acceleration parameter). The threshold of overstabilities is determined in terms of the thermal Rayleigh number as a function of the governing parameters for $\varepsilon = 1$. Mamou and Vasseur [4] reconsider the problem by examining the effect of the enclosure confinement on the onset of overstabilities with $\xi = 0$. A general expression for the thresholds is derived for Dirichlet and Neumann boundary conditions. Following the stability analysis described in Taunton et al. [2], Mamou and Vasseur [4] and Mamou et al. [14], the characteristic equation for the present problem is obtained as follows:

$$\gamma\xi\varepsilon Le\left(\frac{p}{\gamma}\right)^3 + p_2\left(\frac{p}{\gamma}\right)^2 - p_1\left(\frac{p}{\gamma}\right) - p_0 = 0, \tag{19}$$

where

$$p_0 = R_T^0 + R_S^0 - 1, \quad p_1 = \varepsilon Le(R_T^0 - 1) + R_S^0 - 1 - \xi\gamma, \quad p_2 = \varepsilon Le(1 + \xi\gamma) + \xi\gamma, \tag{20}$$

with $R_T^0 = R_T/R^{sup}$ and $R_S^0 = R_S/R^{sup}$. The parameters γ and R^{sup} are defined in Mamou and Vasseur [4].

The threshold of stationary convection ($p = 0$, i.e. $p_0 = 0$) is given by

$$R_{TC}^{sup} = -R_S + R^{sup}. \tag{21}$$

The threshold of overstabilities, which can be obtained by setting $p = ip_i$ (i.e. $p_r = 0$), is

$$R_{TC}^{over} = \mathrm{Min}\left\{ -\frac{\varepsilon Le + \xi\gamma}{\varepsilon^2 Le^2(\xi\gamma + 1)}R_S + \frac{(\varepsilon Le + 1)(\varepsilon Le + \xi\gamma)}{\varepsilon^2 Le^2}R^{sup} \right\} \tag{22}$$

and the corresponding pulsation of the oscillations is given by:

$$p_i^2 = -\gamma^2\frac{p_1}{\varepsilon Le} \quad \text{or} \quad p_i^2 = -\gamma^2\frac{p_0}{p_2}. \tag{23}$$

Nield [1] and Taunton et al. [2] demonstrate (for $\varepsilon = 1$) that the wavelength that minimizes the thresholds of stationary convection and overstabilities is $A_C = 2$ for any value of the governing parameters when $\xi = 0$. However, for $\xi > 0$, Taunton et al. [2] show that the wavelength at the onset of overstabilities ($R_S < 0$) becomes dependent on the governing parameters. The stability diagram, illustrated in Fig. 1, displays the effect of ξ on the critical parameters for $R_S = -100$, $Le = 10$, $\varepsilon = 1$ and $a_T = a_S = 0$. The stable, subcritical, overstable and stationary regimes are delineated in the figure. The wavelength, as shown in Fig. 1(b), decreases slightly, in the close vicinity of $\xi = 0$, and then increases significantly as ξ rises from 0 to 1.2. Fig. 1(a) shows that the increase of ξ delays the appearance of overstabilities. The numerical results show that, for $\xi > 0$, the temperature and concentration perturbation profiles are similar but are shifted in the spatial phase. For Neumann boundary conditions and given set of governing parameters, the onset of overstabilities

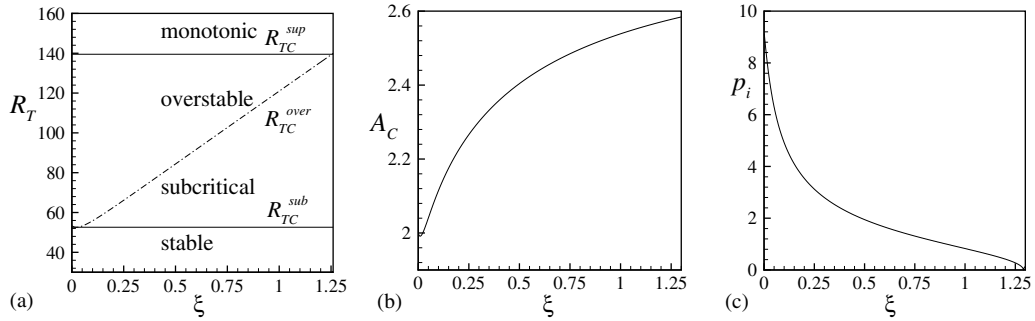

Fig. 1. Stability diagram in the R_T–ξ plane for $Le = 10$, $R_S = -100$, $\varepsilon = 1$ and $a_T = a_S = 0$. The results are obtained with 20 elements in y-direction.

occurs at a zero wavenumber that is independent of the parameter ξ such that the flow remains monocellular for any aspect ratio of the enclosure.

Some relevant features about the instability of thermal convection in horizontal enclosures is now discussed. Kimura et al. [15] claim that the preferable convective mode is the single-cell flow when studying thermal convection in horizontal rectangular enclosures ($A = 10$). Their findings are obtained on the basis of a linear stability analysis that gives a single-cell flow within a rectangular enclosure subject to a constant heat flux, and on their explicit numerical solver for the full governing equations. Their code shows that the solution always converges to monocellular flows for $R_T = 20$. They concluded that the single-cell flow is the unique solution for the problem. Later on, Mamou and Vasseur [4] consider a similar problem and report that when studying double-diffusive convection, single and multi-cellular flows are possible far from criticality. Using different flow solvers and both finite-difference and finite element methods, they find that the single flow is not a unique solution for high Rayleigh number (the results are not presented here). Bénard convection (multi-cellular flows) becomes the preferable flow pattern above a certain value of the thermal Rayleigh number. To confirm these findings, a stability analysis is performed to find which of the possible flow patterns is the preferable convective mode. In the present context, the preferable solution is defined as the one with the higher growth rate. Fig. 2 illustrates the growth rate of different convective modes within a square enclosure for Dirichlet boundary conditions, and within a rectangular enclosure ($A = 10$) for Neumann boundary conditions. For this situation when $\xi = 0$, the growth rate is given by $p_r = \gamma(R_T - R^{sup})/R^{sup}$ by setting the solute buoyancy force to zero ($N = 0$).

For $A = 1$ with $a_T = 0$, $p_r = 0$ corresponds to the threshold of the onset of stationary convection. For one-cell flow, $R^{sup} = 4\pi^2$, and for two-cells flow, $R^{sup} = 25\pi^2/4$. As observed in Fig. 2(a), the growth rates of these two convective modes increase with different slopes as R_T increases. They intersect at $R_T^{int} = 10\pi^2$. Below the intersection point, $R_T = R_T^{int}$, the growth rate of the one-cell mode is higher than that of the two-cell mode. For this situation, the one-cell mode is the preferable one for $R_T < R_T^{int}$. However, for $R_T > R_T^{int}$, the growth rate of the two-cells mode is higher; thus

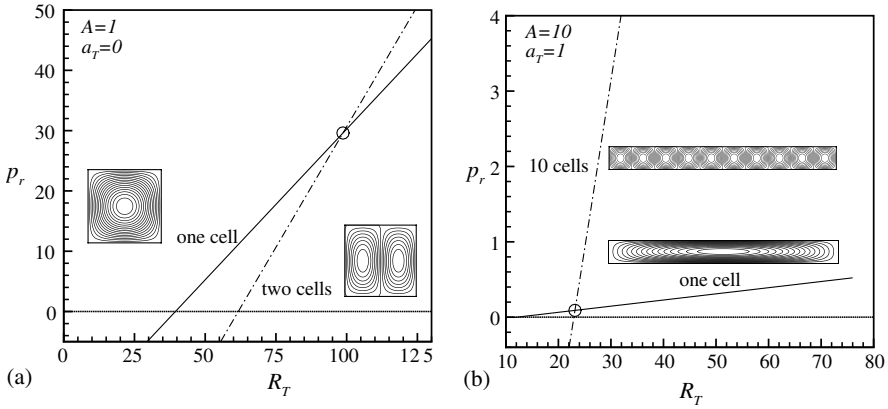

Fig. 2. Growth rate of different convective modes for pure thermal convection: $R_S = 0$, $\xi = 0$ and (a) $A = 1$ with $a_T = 0$, or (b) $A = 10$ with $a_T = 1$. The results are obtained with 12×12 elements for $A = 1$ and 10×20 elements for $A = 10$.

the two-cell mode is the favorable one. It is expected that when solving the governing equations starting with the pure diffusive state as initial conditions, the solution will evolve to one-cell flow for $R_T < R_T^{int}$ and to two-cells flow for $R_T > R_T^{int}$. An hysteresis may exist when transiting between the two modes.

For Neumann boundary conditions, Fig. 2(b), the intersection point between the growth rates for one-cell and 10-cells flow is obtained as $R_T^{int} = 23.15$ (flows with $2, 3, \ldots, 9$ cells are not presented here). The thresholds for stationary convection are $R_{TC}^{sup} = 12.017$ (one-cell flow) and $R_{TC}^{sup} = 22.94$ (10-cells flow). When $R_T > R_T^{int}$, the Bénard convective flow is favorable and the finite amplitude flow may be stable. Also, for $A = 10$, flows with one, two, $\ldots$, 10-cells modes may be possible, providing that the Rayleigh number is sufficiently high.

For mixed boundary conditions, the thresholds of overstabilities and stationary convection are presented in the stability diagram in Fig. 3 for positive thermal Rayleigh numbers (heating from below). The threshold for stationary convection is discussed first. Recall that for pure thermal convection with Dirichlet ($a_T = 0$) and Neumann ($a_T = 1$) boundary conditions, the supercritical Rayleigh numbers, $R_{a_T}^{sup}$ are given by $R_0^{sup} = 4\pi^2$ and $R_1^{sup} = 22.95$, respectively. According to the linear stability results, the flow structure consists of a square single-cell for relatively small solutal Rayleigh numbers $|R_S|$. From the stability diagram, the following relationship were found to fit the threshold of stationary convection curves:

$$R_{TC,(a_T,a_S)}^{sup} = -bR_S + R_{a_T}^{sup}, \quad \text{with } b = \frac{R_{a_T}^{sup}}{R_{a_S}^{sup}} \tag{24}$$

such that, for $(a_T, a_S) = (1, 0)$, $b = -(4\pi^2/22.95) \simeq -1.72$ and for $(a_T, a_S) = (0, 1)$, $b = -(22.95/4\pi^2) \simeq -0.58$.

The above relation is valid as long as the incipient flow remains monocellular and the streamlines circular. As shown in Fig. 3(a), for $(a_T, a_S) = (1, 0)$, the flow patterns are strongly affected by the increase in $|R_S|$. For relatively high solutal Rayleigh numbers $|R_S|$, the circular original cell observed for $R_S \geqslant 0$ is distorted significantly and broken into two co-rotating cells contained within the original cell. One-cell is near the lower boundary and the other near the upper boundary. For large $|R_S|$, a weak recirculation flow is observed between the two-cells. The curves of the threshold for stationary convection are slightly curved due to the change in the flow structure. Similar results have been obtained by Mahidjiba et al. [10].

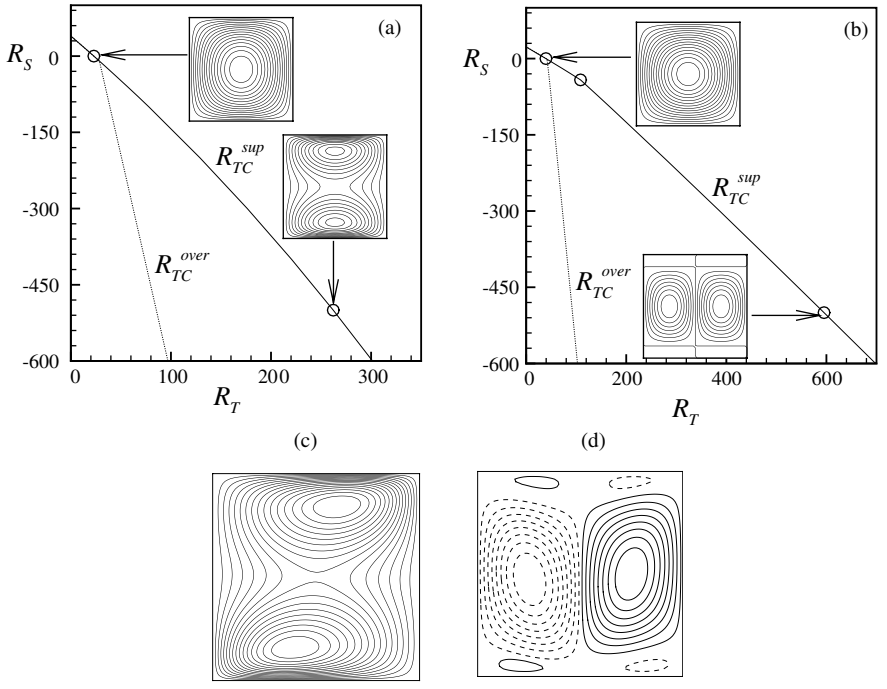

Fig. 3. Stability diagram for mixed boundary conditions within a square enclosure for $\varepsilon = 1$ and $\xi = 0$ with (a) $(a_T, a_S) = (1, 0)$ and (b) $(a_T, a_S) = (0, 1)$. Streamlines for finite amplitude convection for $R_S = -500$ and $Le = 0.5$ and (c) $R_T = 300$ and $(a_T, a_S) = (1, 0)$, $R_{TC}^{sup} = 262.18$; $\Psi_{max} = 0.643$, $\Psi_0 = 0.278$, $Nu_m = 1.098$ and $Sh_m = 1.011$, or (d) $R_T = 650$ and $(a_T, a_S) = (0, 1)$, $R_{TC}^{sup} = 595.20$; $\Psi_{max} = -1.227$, $\Psi_{max} = 1.227$, $Nu_m = 1.190$, $Sh_m = 1.056$. The results are obtained with 40×40 elements.

At the onset of stationary convection, for $(a_T, a_S) = (0, 1)$, the flow pattern is monocellular for $R_S > -41.9$ (see Fig. 3(b)). For $R_S < -41.9$, the flow structure that gives the minimum critical Rayleigh number is characterized by the existence of six convective cells: two main vertical contour-rotating cells (see Fig. 3(b)) occupy the central region of the enclosure and four small cells are located near the top and lower boundaries (i.e. two on the top and two on the bottom). For such boundary conditions, Mahidjiba et al. [10] found that the wavelength decreases to 0.93 within an infinite layer. For the onset of overstabilities, the flow pattern is always monocellular, and as shown in Fig. 3, the threshold of overstabilities obtained for $Le = 10$ is well below the threshold for stationary convection. Finite amplitude flow patterns near the threshold for stationary convection are depicted in Fig. 3(c) and (d) for $(a_T, a_S) = (1, 0)$ and $(a_T, a_S) = (0, 1)$, respectively. The flow patterns are similar to the incipient flow patterns predicted by the linear stability analysis. For $(a_T, a_S) = (0, 1)$, the flow is found to oscillate slightly without noticeable changes in the flow patterns.

4.2. Convective state

The convective solution is obtained analytically for a horizontal infinite layer subject to constant fluxes of heat and solute ($a_T = a_S = 1$). The steady convective solution is expected to become unstable far from the criticality.

4.2.1. Basic convective solution

For a shallow enclosure subject to constant fluxes of heat and solute ($a_T = a_S = 1$), the flow within the enclosure is parallel and the solution is given in Mamou and Vasseur [4].

Typical numerical results obtained by solving the full governing equations (1)–(3) are compared to the analytical solution in Fig. 4. The results are obtained with a grid of 20×120 elements, and $R_T = 100$, $R_S = -100$, $Le = 10$, $A = 10$ and $a_T = a_S = 1$. Fig. 4(a) demonstrates clearly the parallelism of the streamlines with respect to the horizontal walls except in the end regions, and the horizontal linear variations of the temperature and concentration. Fig. 4(b)–(e) illustrate a comparison between the numerical and analytical solutions in terms of the mid-height horizontal and mid-width vertical profiles of Ψ, T and S. There is a good agreement between the two approaches in the central part of the enclosure ($-4 \leqslant x \leqslant 4$).

The analytical solution obtained by Mamou and Vasseur [4] shows that the threshold for stationary convection is given by

$$R_{TC}^{sup} = -R_S + 12. \tag{25}$$

For subcritical flows, the threshold is given by

$$R_{TC}^{sub} = \frac{12}{Le^2}\left(\sqrt{Le^2 - 1} + \sqrt{-R_S/12}\right)^2. \tag{26}$$

For Dirichlet boundary conditions and an infinite layer, Rudraiah et al. [5] determine the threshold of subcritical flows using a weak non-linear stability analysis. The threshold expression is similar to that given in Eq. (26), but with $R^{sup} = 4\pi^2$ instead of 12. Mamou and Vasseur [4] extend the study of Rudraiah et al. [5] by deriving the same expression for general boundary conditions and arbitrary aspect ratio enclosures.

4.3. Onset of transition

The threshold of transition, R_{TC}^{tran}, characterizes the passage from finite amplitude steady convective flows to oscillatory flows. The transition phenomenon occurs usually at high Rayleigh number. The procedure to determine the threshold of transition is the same as that used to compute the threshold of overstabilities for an infinite layer in the previous sections. For this situation, the basic solution Ψ_b, T_b and S_b is given in Mamou and Vasseur [4]. To validate the present numerical procedure, the thermal convection results of Kimura et al. [15] are considered by omitting the solutal buoyancy force ($R_S = 0$) in the present governing equation (13). The critical Rayleigh number for transition is presented in Table 3; the corresponding critical wavenumber k_C and frequency f_r are also displayed in. The results agree well with those obtained by Kimura et al. [15].

The effect of the Lewis number and the normalized porosity on the critical parameters at transition is shown in Fig. 5(a)–(c). The results are presented for $R_S = -100$, $\xi = 0$ and $a_T = a_S = 1$. The parameters ε and Le have a significant effect on the critical parameters. The critical parameters become independent of Le, when Le becomes large enough. This is because of the solute concentration becomes uniform within a large part of the enclosure and the mass transfer is caused mainly by convection. For this situation, the critical values tend towards those corresponding to pure thermal convection. The perturbations profiles at the threshold of transition are depicted in Fig. 5(d)–(e). They consist of small vortices aligned near the horizontal boundaries. Traveling waves can be initiated above the threshold of transition.

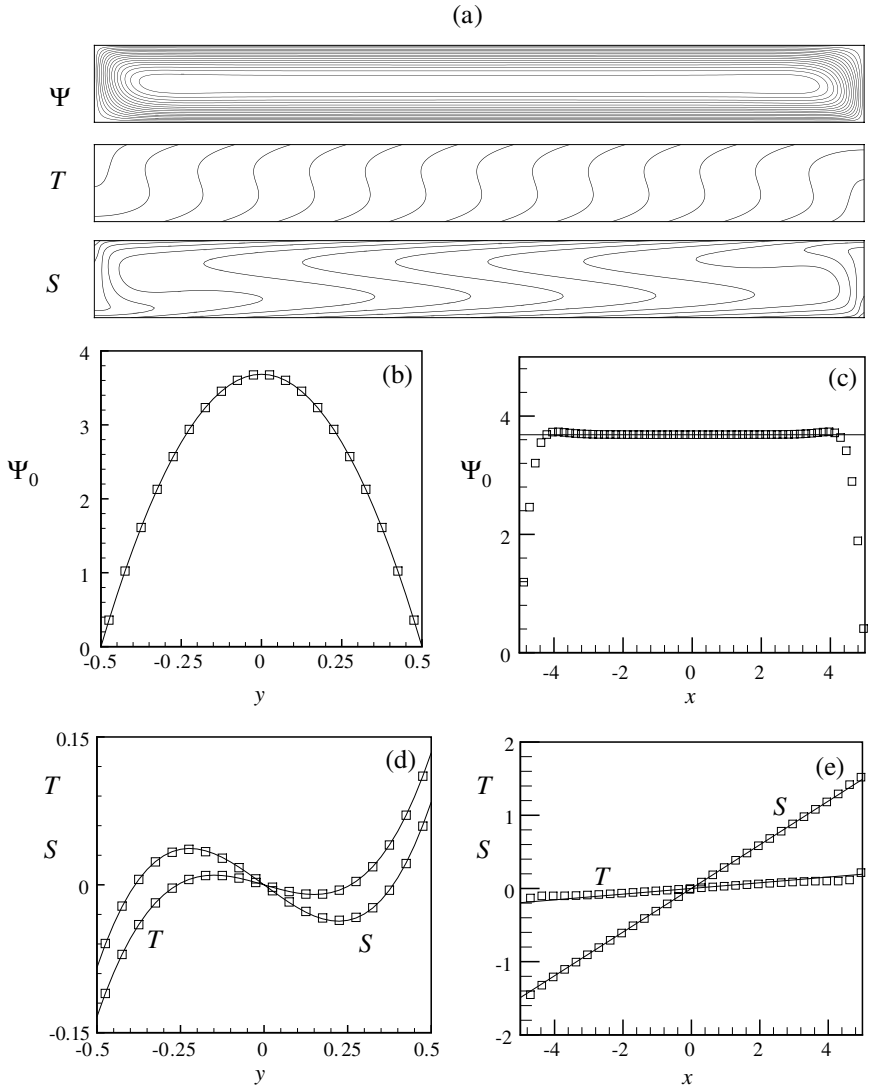

Fig. 4. Comparison between the numerical results and the analytical parallel flow solution for $R_T = 100$, $R_S = -100$, $Le = 10$, $A = 10$ and $a_T = a_S = 1$: (a) streamlines, isotherms and isoconcentrations, (b) vertical stream function profiles at the mid-width and (c) mid-height of the enclosure, and (d) the vertical temperature and concentration profiles at the mid-width and (e) mid-height of the enclosure. Numerical solution: $\Psi_0 = 3.685$, $\Psi_{max} = 3.733$, $Nu = 3.734$, $Nu_m = 3.597$, $Sh = 6.029$ and $Sh_m = 6.726$. Analytical solution: $\Psi_0 = 3.684$, $Nu = Nu_m = 3.734$ and $Sh = Sh_m = 5.959$. The numerical solution is represented by symbols (some symbols are skipped for clarity) and the analytical solution is represented by solid lines. The results are obtained with 20×120 elements.

Table 3
Critical Rayleigh number, R_{TC}^{tran}, critical wavelength, A_C, and oscillation frequency, f_r, at the onset of transition in an infinite layer

Number of elements	4	8	12	16	Kimura et al. [15]
R_{TC}^{tran}	510.0195	506.1841	506.0815	506.0742	506.07
$k_C = 2\pi/A_C$	4.7696	4.8239	4.8257	4.8251	4.825
$f_r = \lvert p_i \rvert/2\pi$	22.0287	22.1070	22.1122	22.1095	22.11

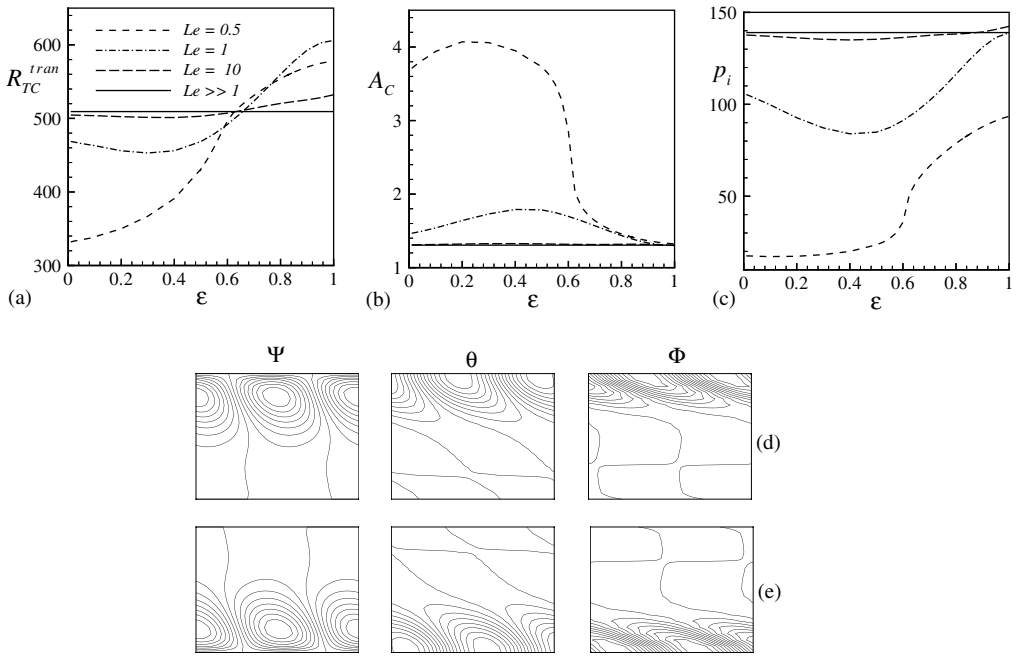

Fig. 5. Effects of Le and ε on the critical parameters at the onset of transition for $R_S = -100$, $a_T = a_S = 1$ and $\xi = 0$: (a) R_{TC}^{tran} versus ε, (b) A_C versus ε, (c) p_{iC} versus ε; and perturbation profiles (ψ, θ and ϕ) at the threshold of transition for $R_S = -100$, $Le = 10$, $\varepsilon = 1$, $\xi = 0$ and $a_T = a_S = 1$: $R_{TC}^{tran} = 532.12$ and $A_C = 1.297$: (d) $p_i = 142.46$, and (e) $p_i = -142.46$. The results are obtained with 20 elements in y-direction.

To examine the oscillatory behavior of the convective flows above the threshold of transition, typical results are presented in Fig. 6 for $R_S = -100$, $Le = 10$, $\varepsilon = 1$, $\xi = 0$ and $(a_T, a_S) = (1, 1)$. The linear stability analysis gives the threshold value of $R_{TC}^{tran} = 532$; the critical wavelength is $A_C = 1.3$. To approximate the flow within an infinite layer, an aspect ratio of $A = 10$ is considered. The amplitude of the oscillations are very small near criticality and changes to the flow pattern are indistinguishable. For this reason, a thermal Rayleigh number of $R_T = 600$ is chosen for the numerical run. For this situation, the flow is periodically oscillating but the flow patterns remain unicellular. However, the parallelism of the streamlines is broken, especially at the mid-height of the enclosure. The unsteadiness of the flow is characterized by the existence of a two superposed layers, each layer consists of a series of secondary circulations traveling in the horizontal direction. The oscillatory behavior of the flow is characterized by periodic locally enhanced heat and mass transfer rates as shown in Fig. 7(c). The extremums of Nu_l and Sh_l follow the vortices as they travel in the horizontal direction. The perturbation flow patterns are displayed in Fig. 7(d) in terms of the perturbed stream function profile ψ_p defined as

$$\psi_p = \Psi - \frac{1}{\tau}\int_0^\tau \Psi \, dt. \tag{27}$$

The vortices in both the two layers are seen to travel along the enclosure walls in the clockwise direction. As shown in Fig. 7(c) and (d), the vortices strengthen as they approach the vertical walls and the heat and mass transfer rates becomes enhanced near the end regions of the enclosure. The shape and wavelength of the formed vortices are approximately the same as those predicted by the stability analysis when superposing the two conjugate solutions.

The effect of the acceleration parameter, ξ, on the threshold of transition is also studied for the same problem. Typical results are depicted in Table 4 for $R_S = -100$, $Le = 10$, $\varepsilon = 1$ and $(a_T, a_S) = (1, 1)$. When ξ increases, the threshold for transition is delayed and the perturbation wavelength becomes large. The oscillation frequency (i.e. pulsation) also decreases. As a result, the steady-state flows can be stabilized by increasing ξ.

The bifurcation diagram is given in Fig. 7 for $R_T = 100$, $R_S = -100$, $Le = 10$, $A = 10$ and $a_T = a_S = 1$. The results are presented in terms of the local heat and mass transfer rates (Nu and Sh) as a function of the thermal Rayleigh number. Five modes are shown on the graph. The first one, Region I, corresponds to the stable diffusive regime in which all perturbations decay. Region II corresponds to subcritical flows where the diffusive state is unstable to finite amplitude perturbations. Region III is the overstable regime in which perturbations grow in an oscillatory manner. The

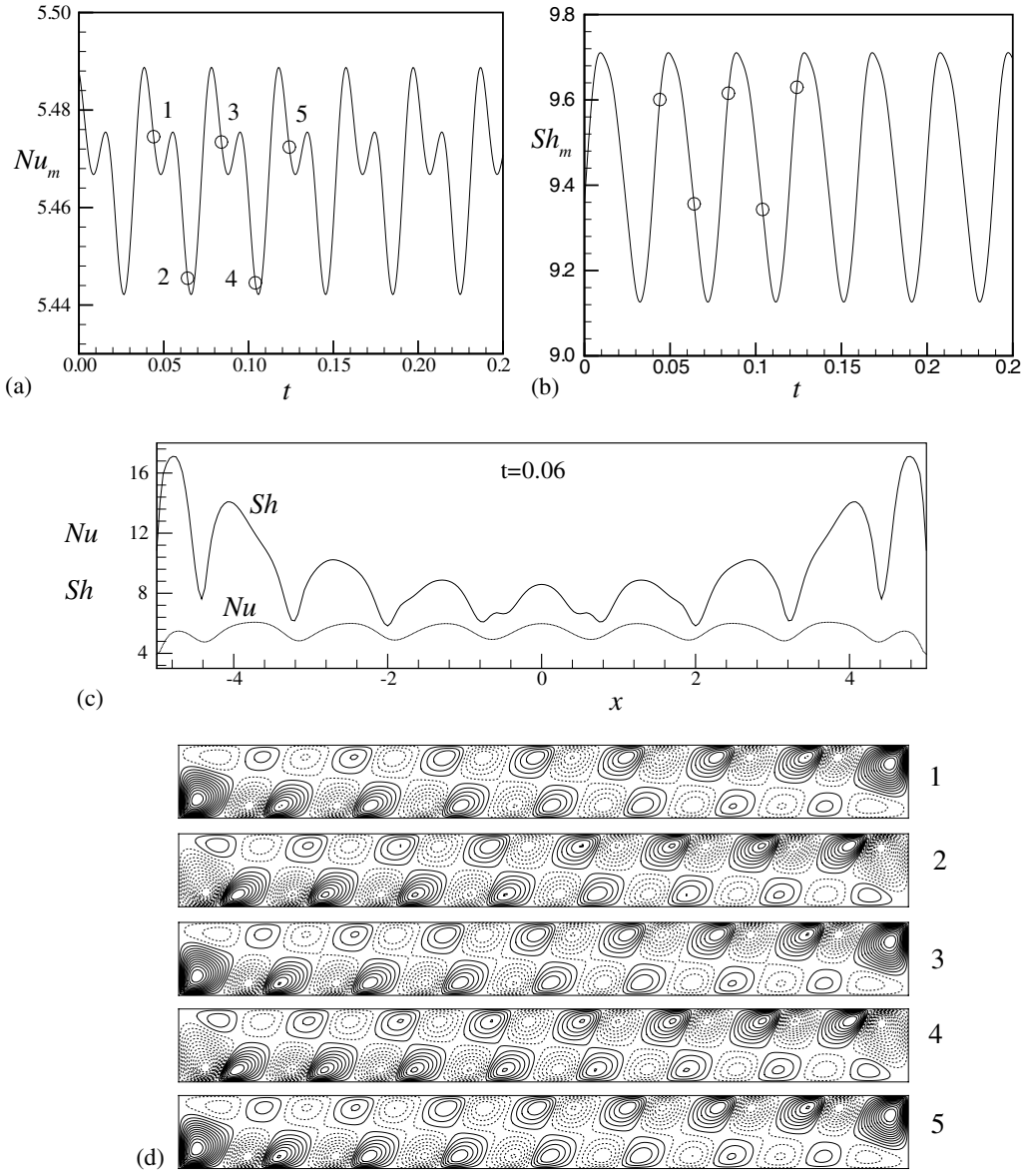

Fig. 6. Time history of the (a) heat and (b) mass transfer rates; (c) streamlines, temperature, solute and perturbed stream function contours at $t = 0.785$. $R_T = 600$, $R_S = -100$, $Le = 10$, $A = 10$, $\varepsilon = 1$, $\xi = 0$ and $a_T = a_S = 1$. The results are obtained with 20×120 elements and a time step of $\Delta t = 5 \times 10^{-5}$.

overstable regime extent to R_{TC}^{osc} above the oscillation frequency vanishes. Region IV represents the stationary convection regime, and region V corresponds to the oscillatory finite amplitude convection that occurs right above the threshold of transition.

In metallurgy, many crystal growth systems, such as the solidification of metallic alloys or binary mixtures, the region (interface) separating the solid and the liquid regions consists of a mixture of liquid and crystals (solid matrix). The region is known as a mushy layer, in which the flow can be described by Hazen–Darcy law, Chung and Worster [16]. When the mushy layer is horizontal, the temperature gradient and the solute gradient due to mass rejection at the interface can trigger convective instabilities with/without formation of chimneys due to difference in thermal and solute diffusion. In such systems, the prediction of steady or oscillatory convective flows is very important since they can lead

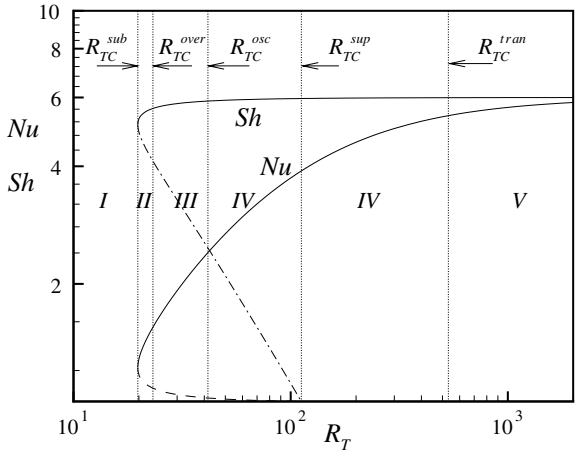

Fig. 7. Bifurcation diagram (*Nu* and *Sh* versus R_T) for $R_T = 100$, $R_S = -100$, $Le = 10$, $A = 10$ and $a_T = a_S = 1$. The critical parameters are obtained for $\xi = 0$ and $\varepsilon = 1$ as: $R_{TC}^{sub} = 19.8$, $R_{TC}^{over} = 23.2$, $R_{TC}^{osc} = 41.6$, $R_{TC}^{sup} = 112.0$ and $R_{TC}^{tran} = 532.1$.

Table 4
Effect of the acceleration parameter ξ on the threshold of transition in an infinite layer: $Le = 10$, $R_S = -100$, $\varepsilon = 1$ and $(a_T, a_T) = (1, 1)$

ξ	R_{TC}^{tran}	A_C	p_i
0	532.12	1.30	±142.46
10^{-3}	521.19	1.38	±128.10
2×10^{-3}	526.25	1.49	±115.37
5×10^{-3}	583.69	1.91	±91.48
10^{-2}	748.39	2.60	±74.19
2×10^{-2}	1360.71	4.02	±62.68

to non-uniform crystal growth and undesirable non-homogeneous crystals. The behavior of the diffusion and the convective flows described in the present study are comparable to the practical situation described in [16].

5. Conclusions

In the present work, a thorough investigation is conducted on the stability of the rest and convective states within a shallow porous layer subject to vertical thermal and solutal gradients. The governing equations are solved numerically using the finite element method. Based on linear stability theory, the resulting linear perturbed equations are solved numerically also using the finite element method. Considering different thermal and solutal boundary conditions, the threshold for the onset of overstability and the threshold of transition are determined as functions of the governing parameters. The latter characterizes the transition from steady to oscillatory convective flows. Both thresholds depend considerably on the acceleration coefficient and the normalized porosity of the porous material. An increase in the two parameters delays the appearance of overstabilities and finite amplitude oscillatory convection. The wavenumber at criticality depends on this two parameters.

At the onset of overstabilities, the wavenumber $k_C = \pi$ is constant and independent of the governing parameters when the acceleration parameter is zero. However, the wavenumber becomes a function of the governing parameter when the acceleration is finite. At the onset of stationary convection, the wavelength is constant $k_C = \pi$ for Dirichlet thermal and solutal boundary conditions and zero for Neumann boundary conditions. For mixed boundary conditions, the wavenumber remains a function of the governing parameters. For a square enclosure and relatively small solutal Rayleigh numbers, the threshold for stationary convection is given by $R_{TC}^{sup} = -1.72R_S + 22.95$ when the enclosure was subject to Neumann thermal and Dirichlet solutal boundary conditions, and by $R_{TC}^{sup} = -0.58R_S + 4\pi^2$ for Dirichlet thermal and Neumann solutal boundary conditions.

Acknowledgements

The author is grateful to the National Research Council for providing facilities for word processing and printing the paper. The author thanks Dr. S. McIlwain for reviewing this paper and for providing fruitful comments.

References

[1] D.A. Nield, Onset of thermohaline convection in porous medium, Water Resour. Res. 4 (1968) 553–560.
[2] J.W. Taunton, E.N. Lightfoot, T. Green, Thermohaline instability and salt fingers in a porous medium, Phys. Fluids 15 (1972) 748–753.
[3] M. Mamou, P. Vasseur, E. Bilgen, D. Gobin, Double-diffusive convection in an inclined slot filled with porous medium, Eur. J. Mech. B/Fluids 14 (1995) 629–652.
[4] M. Mamou, P. Vasseur, Thermosolutal bifurcation phenomena in porous enclosures subject to vertical temperature and concentration gradients, J. Fluid Mech. 395 (1999) 61–87.
[5] N. Rudraiah, P.K. Shrimani, R. Friedrich, Finite amplitude convection in a two-component fluid saturated porous layer, Int. J. Heat Mass Transfer 25 (1982) 715–722.
[6] H. Brand, V. Steinberg, Nonlinear effects in the convective instability of a binary mixture in a porous medium near threshold, Phys. Lett. 93A (1983) 333–336.
[7] B.T. Murray, C.F. Chen, Double-diffusive convection in a porous medium, J. Fluid Mech. 201 (1989) 147–166.
[8] F. Chen, C.F. Chen, Double-diffusive fingering convection in a porous medium, Int. J. Heat Mass Transfer 36 (1993) 793–807.
[9] A. Amahmid, M. Hasnaoui, M. Mamou, P. Vasseur, Double-diffusive parallel flow induced in a horizontal brinkman porous layer subjected to constant heat and mass fluxes: analytical and numerical studies, Heat Mass Transfer 35 (1999) 409–421.
[10] A. Mahidjiba, M. Mamou, P. Vasseur, Onset of double-diffusive convection in a rectangular porous cavity subject to mixed boundary conditions, Int. J. Heat Mass Transfer 43 (2000) 1505–1522.
[11] L. Kalla, M. Mamou, P. Vasseur, L. Robillard, Multiple solutions for double diffusive convection in a shallow porous cavity with vertical fluxes of heat and mass, Int. J. Heat Mass Transfer 44 (2001) 4493–4504.
[12] M. Mamou, P. Vasseur, E. Bilgen, Double diffusive convection instability problem in a vertical porous enclosure, J. Fluid Mech. 368 (1998) 263–289.
[13] M. Mamou, P. Vasseur, E. Bilgen, A Galerkin finite-element study of the onset of double-diffusive convection in an inclined porous enclosure, Int. J. Heat Mass Transfer 41 (1998) 1513–1529.
[14] M. Mamou, P. Vasseur, M. Hasnaoui, On numerical stability analysis of double-diffusive convection in confined enclosures, J. Fluid Mech. 433 (2001) 209–250.
[15] S. Kimura, M. Vynnycky, F. Alavyoon, Unicellular natural circulation in a shallow horizontal porous layer heated from below by a constant flux, J. Fluid Mech. 294 (1995) 231–257.
[16] C.A. Chung, M.G. Worster, Steady-state chimneys in a mushy layer, J. Fluid Mech. 455 (2002) 387–411.